The validity of the Kirchhoff approximation for rough surface scattering using a Gaussian roughness spectrum

Eric I. Thorsos

Citation: The Journal of the Acoustical Society of America **83**, 78 (1988); doi: 10.1121/1.396188
View online: https://doi.org/10.1121/1.396188
View Table of Contents: https://asa.scitation.org/toc/jas/83/1
Published by the Acoustical Society of America

The validity of the Kirchhoff approximation for rough surface scattering using a Gaussian roughness spectrum

Eric I. Thorsos
Applied Physics Laboratory, College of Ocean and Fishery Sciences, University of Washington, Seattle, Washington 98105

(Received 4 May 1987; accepted for publication 15 September 1987)

The validity of the Kirchhoff approximation for rough surface scattering is examined by comparison with exact results obtained by solving an integral equation. The pressure release boundary condition is assumed. The field quantity calculated is the bistatic scattering cross section, which is obtained with a Monte Carlo technique. The accuracy of correcting the Kirchhoff scattering cross section for shadowing is also addressed. The surface realizations used are randomly rough with a Gaussian roughness spectrum and have height variations in only one direction. The surface correlation length is found to be the most important parameter in defining the valid region of the Kirchhoff approximation away from the low grazing angle region. A procedure is given that provides a quantitative measure of the accuracy of the shadow-corrected approximation when the root-mean-square (rms) slope angle of the surface γ is $\lesssim 20°$ and when the incident grazing angle θ is $\gtrsim 2\gamma$. Examples with $\theta \lesssim 2\gamma$ are also discussed.

PACS numbers: 43.30.Gv, 43.30.Hw

INTRODUCTION

There are two well-known theoretical methods for calculating acoustic scattering from rough surfaces. One is based on the small roughness perturbation approximation[1,2] (also known as the Rayleigh–Rice approximation) and the other is based on the Kirchhoff (or physical optics) approximation.[3,4] The perturbation approach is valid when the root-mean-square (rms) surface height h is small compared with the acoustic wavelength λ. It has been applied, for example, to low-frequency acoustic scattering from the sea surface where the validity condition can be satisfied.[2,5] The valid region of the Kirchhoff approximation, on the other hand, is not well established. The Kirchhoff approximation is generally assumed to apply to "gently undulating" surfaces—more specifically, to surfaces with radius of curvature large compared with a wavelength. Since the Kirchhoff approximation is not restricted to small values of h/λ, it has been developed for applications in the moderate-to-high frequency range.[6,7] Scattering at low grazing angles is of obvious practical importance in underwater acoustics, yet the Kirchhoff approximation is usually considered suspect at low grazing angles and for backscattering in general. No procedure has existed for estimating the conditions for which the error in the scattered intensity would exceed some prescribed value, such as 1 or 2 dB. Therefore, the applicable region of the Kirchhoff approximation has remained uncomfortably nebulous.

In this paper, the accuracy of the Kirchhoff approximation for randomly rough pressure release surfaces is examined through comparison with "exact" numerical results. The exact solution for the bistatic[8] scattered field is found using an integral equation technique similar to that used by Lentz[9] and Axline and Fung.[10] The solutions are exact in the sense that no approximations are made in the scattering physics: Effects of multiple scattering and shadowing, for example, are automatically included. Two independent solution methods have been developed and the results compared for consistency. Error arising from the discretization of the integral equation has been shown to be negligible by variation of the partition width. Computer limitations restrict this work to surfaces that are rough in one direction only (1-D surfaces), i.e., to a scattering problem in two space dimensions. Such studies can nevertheless be expected to give valuable insight into the full 3-D surface scattering problem.

For the present work, a Gaussian roughness spectrum is used. The Gaussian spectrum falls off at high spatial wavenumbers more rapidly than power law spectra, which are more typical of rough surfaces found in nature. The Gaussian choice is a useful simplification because it restricts the roughness to a single spatial scale. Power law spectra are multiscale, which complicates the rough surface scattering problem. There are composite roughness models for the multiscale case[11,12] that combine the Kirchhoff and perturbation approximations into one model, but the Gaussian spectrum provides a less complicated environment for investigating the breakdown of scattering theory approximations.

The surface height and slope distributions are also assumed to be Gaussian. Attention is restricted to surface rms slope angles of less than 20°, which covers most cases of practical interest. The examples considered here correspond roughly to sea surface scattering in the few hundred hertz region. The values of l/λ used here, where l is the surface correlation length, are about the same for sea surface scattering with roughness produced by modest wind speeds ($\lesssim 10$ m/s). The examples studied have higher rms slopes than the sea surface, causing shadowing effects to extend to higher grazing angles. For the results discussed, $0.45 \leqslant l/\lambda \leqslant 4.75$ and $0.053 \leqslant h/\lambda \leqslant 0.701$.

The field quantity calculated in this work is the bistatic scattering cross section σ (per unit surface length per unit scattered angle), which is obtained with a Monte Carlo tech-

 0001-4966/88/010078-15$00.80

nique. For each case, 50 surface realizations consistent with the Gaussian spectrum are generated. The scattered intensity in the farfield, which is a function of the scattering angle for a specified incident angle, is computed numerically for each realization using the integral equation method. The scattering cross section and the scattering strength defined by $10 \log \sigma$ are found from the average scattered intensity. A similar Monte Carlo computation is then done for comparison using the Kirchhoff approximation. The standard Kirchhoff approximation cross section is also calculated—that is, the ensemble averaging is performed theoretically using the statistical properties of the surfaces; this approach avoids the Monte Carlo method.

It is well known that effects of shadowing must be taken into account in calculating the scattering cross section, both for low incident grazing angles (incident field shadowing) and for low scattered grazing angles (scattered field shadowing). The Kirchhoff approximation does not account for shadowing. Corrections for shadowing are available from the literature,[13] but they are based on the high-frequency limit, or geometric optics, approximation and do not account for diffraction or other finite wavelength effects. The accuracy of correcting the Kirchhoff scattering cross section, which does include diffraction, with a shadowing theory based on geometric optics is an open question. Establishing the accuracy of the shadow-corrected Kirchhoff cross section is therefore an important part of this work.

The goal of the present study is to clarify the conditions under which the Kirchhoff approximation (or Kirchhoff approximation with shadowing correction) fails for a Gaussian roughness spectrum and to give a quantitative procedure for estimating the error when the error is modest. The general problem is simplified here in several respects. First, the rms slope angle γ of the surface is chosen to be $\lesssim 20°$. Second, we concentrate on relatively large incident grazing angles θ, where $\theta \gtrsim 2\gamma$.

The main results are as follows. In general, the ratio of surface correlation length l to acoustic wavelength λ is the key surface parameter in determining the validity of the Kirchhoff approximation. This is in contrast to the commonly held view that the ratio of the radius of curvature to the acoustic wavelength is the important parameter. The validity of the Kirchhoff approximation depends in addition on the relationship between the incident and scattered grazing angles and the rms slope (or effective rms slope, to be defined later); this dependence can be readily associated with shadowing or multiple scattering effects.

The Kirchhoff approximation has been found to be in error under two sets of conditions when $\theta \gtrsim 2\gamma$. First, for $l/\lambda \gtrsim 1$, the only significant error in the Kirchhoff cross section appears to be related to shadowing of the scattered field, but it is not completely accounted for by standard shadowing theory. When shadowing is not important, the Kirchhoff approximation is accurate; this includes the bistatic backscatter region. Comparisons with exact results show the apparent shadowing correction to be greater than that given by geometric optics theory. Second, as l/λ decreases below 1, shadowing corrections are still needed, but the Kirchhoff approximation yields progressively higher scattering cross sections relative to the exact result for bistatic backscatter. The error occurs in such a way that use of an effective correlation length $l' > l$ in the Kirchhoff calculation yields good agreement with exact results. The appropriate value of l' depends on l, but appears independent of incident grazing angle ($\theta \gtrsim 20°$) and rms surface slope ($\gamma \lesssim 20°$).

Simple algorithms are proposed to indicate when the standard Kirchhoff scattering cross section plus shadowing correction is accurate to within about 1 dB for the parameters studied.

The situation for incident grazing angles lower than $\sim 2\gamma$ is also briefly discussed. The bistatic backscatter region can be assessed using the same algorithms as above, but the forward scatter region is more complicated. It appears that for these conditions shadowing is not sufficient to account for the full effect of multiple scattering. The lower grazing angle region is the subject of further study.

Section I provides details of the exact scattering computation. In Sec. II, numerical examples are given that introduce the various computations used in Sec. III to analyze the Kirchhoff approximation. Results are summarized in Sec. IV.

I. NUMERICAL METHOD

There are several approaches for calculating scattering from 1-D surfaces exactly. A number of investigators[14–18] have studied sinusoidal and other periodic surfaces using methods that exploit periodicity. These calculations can also be made without invoking periodicity by using surfaces of finite length, as was done, for example, by Fung and coworkers for scattering from randomly rough surfaces.[10,19,20] The latter method is used in the present work. The incident field is chosen to fall off smoothly near the ends of the finite length surface segment, thereby avoiding edge effects (Sec. I C). This method can be cast into two formally equivalent forms (using linear integral equations of the first or second kind), both of which are numerically well conditioned. This provides a very useful numerical check.

A. Integral equations

The Helmholtz integral formula is our starting point for obtaining the exact solution to scattering from a 1-D surface with free-surface boundary conditions. Using this formula, we can write the total acoustic pressure $p(\bar{r})$ that results from an incident field $p_{\text{inc}}(\bar{r})$ interacting with a rough surface S as[21]

$$p(\bar{r}) = p_{\text{inc}}(\bar{r}) - \frac{1}{4i}\int_s H_0^{(1)}(k\,|\bar{r}-\bar{r}'|)\frac{\partial p(\bar{r}')}{\partial n'}\,ds' . \tag{1}$$

In Eq. (1), $H_0^{(1)}$ is the zero-order Hankel function of the first kind, k is the acoustic wavenumber, and $\partial p(\bar{r})/\partial n$ is the (unknown) normal derivative of the total pressure on the surface.

Two integral equations can be developed for $\partial p(\bar{r})/\partial n$. By letting $\bar{r}$ approach the surface and using the boundary condition that $p(\bar{r}) = 0$ on the surface, we have

$$p_{\text{inc}}(\bar{r}) = \frac{1}{4i}\int_s H_0^{(1)}(k\,|\bar{r}-\bar{r}'|)\frac{\partial p(\bar{r}')}{\partial n'}\,ds' , \tag{2}$$

with both $\bar{r}$ and $\bar{r}'$ confined to the surface. Equation (2) is a linear integral equation of the first kind for $\partial p(\bar{r})/\partial n$.

Alternately, we can apply the operator $\partial/\partial n = \hat{n}\cdot\bar{\nabla}$ to (1), with $\hat{n}$ the outward normal (Fig. 1) and then take the limit as $\bar{r}$ approaches the surface. As discussed by Meecham,[22] special care is required in moving $\partial/\partial n$ inside the integral in the limit as $\bar{r}$ approaches the surface. The result is

$$\frac{\partial p(\bar{r})}{\partial n} = 2\frac{\partial p_{\text{inc}}(\bar{r})}{\partial n} - \frac{1}{2i}\int_s \frac{\partial}{\partial n} \times H_0^{(1)}(k|\bar{r}-\bar{r}'|)\frac{\partial p(\bar{r}')}{\partial n'}\,ds' . \tag{3}$$

Equation (3) is a linear integral equation of the second kind for $\partial p(\bar{r})/\partial n$. After finding $\partial p(\bar{r})/\partial n$ from either (2) or (3), the scattered field $p_s(\bar{r}) = p(\bar{r}) - p_{\text{inc}}(\bar{r})$ then follows from (1).

The integral equations are solved using a quadrature method. The integration variable is transformed to the x coordinate using $ds' = \gamma(x')dx'$ with $\gamma^2(x') = 1 + [df(x')/dx']^2$, where $f(x)$ is the surface height function. The integral equations are converted to matrix equations by partitioning the surface into N subintervals of length $\Delta x = L/N$, with L the total surface length. Equation (2) becomes a matrix equation of the form

$$a_m = \sum_{n=1}^{N} A_{mn}\, b_n , \quad m = 1,\ldots,N, \tag{4}$$

with

$$a_m = p_{\text{inc}}(\bar{r}_m) ,$$
$$A_{mn} = \begin{cases} H_0^{(1)}(k|\bar{r}_m - \bar{r}_n|) , & m \neq n, \\ H_0^{(1)}[(k\Delta x/2e)\gamma_m] , & m = n, \end{cases} \tag{5}$$

and

$$b_n = \frac{\Delta x}{4i}\gamma_n \left.\frac{\partial p(\bar{r}')}{\partial n'}\right|^{\bar{r}_n},$$

where $\bar{r}_m = x_m\hat{x} + f(x_m)\hat{z}$, $x_m = (m - \frac{1}{2})\Delta x - L/2$, and $\gamma_m = \gamma(x_m)$. Similarly, Eq. (3) can be cast into the form of Eq. (4) with

$$a_m = \left.\frac{\partial p_{\text{inc}}}{\partial n}\right|^{\bar{r}_m},$$
$$A_{mn} = \begin{cases} \left.\dfrac{\partial H_0^{(1)}(k|\bar{r}-\bar{r}_n|)}{\partial n}\right|^{\bar{r}=\bar{r}_m}, & m \neq n, \\ i\left(\dfrac{2}{\Delta x\gamma_m} - \left.\dfrac{d^2 f}{dx^2}\right|^{x_m} \Big/ \pi\gamma_m^3\right), & m = n, \end{cases} \tag{6}$$

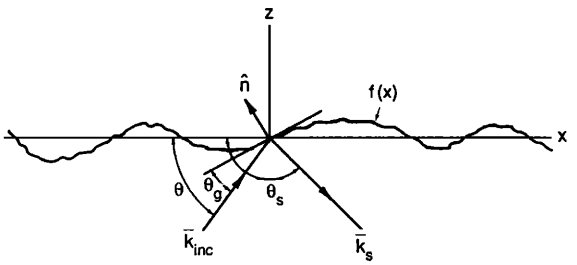

FIG. 1. Scattering geometry.

and with b_n as above. Note that A_{mn} is symmetric for the integral equation of the first kind, Eq. (5). It can be shown from Eq. (6) that A_{mn} is not symmetric for the integral equation of the second kind; therefore, using Eq. (5) is more efficient computationally.

The diagonal matrix elements require special treatment. In Eq. (2), $H_0^{(1)}(k|\bar{r}-\bar{r}'|)$ has an integrable (weak) singularity at $\bar{r} = \bar{r}'$. Thus we use

$$A_{mm} = \int_{x_m - \Delta x/2}^{x_m + \Delta x/2} H_0^{(1)}(k|\bar{r}_m - \bar{r}'|)\frac{dx'}{\Delta x}. \tag{7}$$

The expression for A_{mm} in (5) follows from (7) when the small argument expansion for $H_0^{(1)}$ is used. In (6) the first term in A_{mm} originates from the left-hand side of (3). The second term follows from evaluating

$$\frac{\partial}{\partial n} H_0^{(1)}(k|\bar{r}-\bar{r}'|)$$

at $\bar{r} = \bar{r}'$ using a Taylor series expansion of $f(x')$ about x.

The solution vector b_n for the linear system (4) has been found using LINPACK routines.[23] Values of N up to 400 have been used on a VAX 11/750 and values up to 800 have been used on a CRAY X-MP/48. All cases to date have been numerically well conditioned. Use of $\Delta x = \lambda/5$ gives energy conservation to within about 1% for the examples discussed here.

The scattered field is needed in the farfield for computation of the scattering cross section. With the aid of the farfield form

$$H_0^{(1)}(k|\bar{r}-\bar{r}'|) \sim (2/\pi k)^{1/2} e^{-i\pi/4}(e^{ikr}/\sqrt{r})\, e^{-i\bar{k}_s\cdot\bar{r}'},$$

where $\bar{k}_s = k\bar{r}/r$ and $r = |\bar{r}|$, the scattered field is obtained from (1) as

$$p_s(\bar{r}) = -\left(\frac{2}{\pi k}\right)^{1/2} e^{-i\pi/4}\frac{e^{ikr}}{\sqrt{r}}\sum_{n=1}^{N} e^{(-i\bar{k}_s\cdot\bar{r}_n)} b_n . \tag{8}$$

As an alternative to the procedure outlined above, it is also possible to apply the techniques developed for periodic surfaces to randomly rough surfaces by extending the random surfaces periodically. In this approach, the unknown surface field (the normal derivative of the pressure on the surface, or equivalently the normal derivative of the velocity potential) is usually expanded in a set of periodic basis functions and a matrix equation developed for the unknown coefficients. Work by Chuang and Kong[16] indicates that at least some expansion methods become numerically ill conditioned for sufficiently large surface slopes. The method used in the present work has no apparent limitation on surface slope although it is possibly more intensive computationally than the expansion technique. In addition, using a finite length surface segment (as opposed to its periodic extension) yields a scattering cross section that is a continuous function of the scattered angle and does not exhibit the discrete grating-type angular behavior characteristic of scattering from periodic surfaces. The continuous cross section is convenient for comparision with approximate theoretical methods applied to randomly rough surfaces.

B. Incident field

In the scattering computation, we must guard against edge effects, that is, scattering from the ends of the surface realizations. For nonperiodic surfaces, this can be accomplished by tapering a plane wave to negligible levels at the ends of each surface segment. As a result, the incident field cannot be expressed as a single plane wave, but instead contains a narrow angular distribution of energy about the mean incident grazing angle. A common means of applying such a "beam pattern" to the incident field is to use a Gaussian taper function yielding

$$p_{\rm inc}(\bar{r}) = \exp[i\bar{k}_{\rm inc}\cdot\bar{r} - (x - z\cot\theta)^2/g^2]\,, \qquad (9)$$

where θ is the mean grazing angle of the incident field, $\bar{k}_{\rm inc} = k(\cos\theta\hat{x} + \sin\theta\hat{z})$, and g is the parameter that controls the tapering.

Although expressions equivalent to (9) are often used and are suitable for many applications, $p_{\rm inc}(\bar{r})$ as given by (9) is only an approximate solution to the Helmholtz equation

$$(\nabla^2 + k^2)p(\bar{r}) = 0\,, \qquad (10)$$

as can be verified readily. Consequently, (9) is only an approximation to the actual field, that is, the field corresponding to the boundary value $p_{\rm inc}(\bar{r})|^{z=f(x)}$; thus $\partial p_{\rm inc}(\bar{r})/\partial n|^{z=f(x)}$ and $p_{\rm inc}(\bar{r})|^{z=f(x)}$ are not completely consistent. This effect shows up when detailed comparisons are made between the solutions obtained with (2) and (3) using (9). These solutions can be brought into essentially exact agreement by using a modified form of (9);

$$p_{\rm inc}(\bar{r}) = \exp\{i\bar{k}_{\rm inc}\cdot\bar{r}[1 + w(\bar{r})] - (x - z\cot\theta)^2/g^2\}\,, \qquad (11)$$

where $w(\bar{r}) = [2(x - z\cot\theta)^2/g^2 - 1]/(kg\sin\theta)^2$. A corresponding expression for $\partial p_{\rm inc}(\bar{r})/\partial n$ follows readily from (11). Again, g controls the tapering and $g = L/4$ has been found to be acceptable. The presence of the $w(\bar{r})$ term in (11) ensures that $p_{\rm inc}(\bar{r})$ satisfies the wave equation to order $1/(kg\sin\theta)^2$, where $kg\sin\theta \gg 1$.

An alternate form of $p_{inc}(\bar{r})$, which satisfies the wave equation exactly, is given in the Appendix, together with a derivation of Eq. (11), which is a more convenient form to use. Comparisons of the integral equation solutions using (11) and the form in the Appendix show (11) to be fully adequate for the cases discussed in this paper. The finite angular width of the incident field is also discussed in the Appendix.

C. Scattering cross section

The results of the scattering calculations will be presented in terms of the scattering strength defined by

$$\mathrm{SS} = 10\log\sigma(\theta,\theta_s), \qquad (12)$$

where $\sigma(\theta,\theta_s)$ is the dimensionless scattering cross section per unit scattered angle per unit surface length. For a plane wave incident on a surface of length L, the cross section for a 2-D scattering geometry (1-D surface) is defined by

$$\sigma(\theta,\theta_s) = \langle I_s\rangle r/I_{\rm inc}L = \langle I_s\rangle r\sin\theta/E_f\,, \qquad (13)$$

where $I_{\rm inc}$ is the incident intensity, $\langle I_s\rangle$ is the scattered intensity for the scattered angle θ_s at the farfield range r averaged over surface realizations, and E_f is the energy flux through the surface. For a tapered incident field, we define the cross section by the expression on the right-hand side in (13) and compute the energy flux[24] using (11) to obtain

$$\sigma(\theta,\theta_s) = \langle|p_s(\bar{r})|^2\rangle r/\{\sqrt{\pi/2}g[1 - 0.5(1 + 2\cot^2\theta)/(kg\sin\theta)^2]\}\,. \qquad (14)$$

For all the examples discussed in this paper, the term of order $(kg\sin\theta)^{-2}$ is $\ll 1$ and could be neglected; it is included for completeness. This also applies to Eq. (24).

We shall see in Secs. II and III that use of the tapered incident field does not lead to a significant difference between the Kirchhoff approximation results obtained with the Monte Carlo method and those obtained with the standard calculation, which assumes a plane wave incident on arbitrarily long surfaces. This is a good indication that the cross section given by (14) can be compared with plane-wave results for the examples given in this article.

The cross section in (14) is the total scattering cross section, accounting for both the coherent and incoherent scattered energy. It is easy to show from Eq. (13) that σ integrated over all θ_s must reduce to $\sin\theta$ in order for energy to be conserved.

D. The Kirchhoff approximation

To obtain the Kirchhoff approximation, we begin with Eq. (3) and drop the second term on the right-hand side:

$$\frac{\partial p(\bar{r})}{\partial n} \cong 2\frac{\partial p_{\rm inc}(\bar{r})}{\partial n}\,. \qquad (15)$$

Because Eq. (15) is exact for a flat surface, the Kirchhoff approximation amounts to using a value for $\partial p(\bar{r})/\partial n$ that would be correct for reflection from a plane tangent to the surface at point $\bar{r}$. Hence, it is also called the "tangent plane" approximation. Intuitively, the Kirchhoff approximation would appear to be appropriate when the surface is "locally planar" on the scale of an acoustic wavelength or, equivalently, when the surface radius of curvature is large compared with a wavelength. We shall see, however, that this description is not very useful for assessing the accuracy of the approximation.

Monte Carlo Kirchhoff results are obtained by using (15) in (1), where the same partitioning is used as with the integral equations. The scattering strength is then calculated as before. Of course, with the Kirchhoff approximation the Monte Carlo approach is unnecessary and is done here for comparison purposes only. Standard methods exist for computing the average scattering cross section from randomly rough surfaces using the Kirchhoff approximation. This theoretical Kirchhoff prediction will also be discussed in Secs. II and III.

E. Random surface generation

For each Monte Carlo run, 50 surface realizations are generated using a spectral method.[25] The object is to generate realizations of the surface height function $f(x)$ consis-

tent with a given roughness spectrum and obeying Gaussian statistics, i.e., having Gaussian distributed heights and slopes. We begin with a surface roughness spectral density $W(K)$ normalized such that

$$\int_{-\infty}^{\infty} W(K)dK = h^2,$$

where h^2 is the mean-square surface height and K denotes the surface spatial wavenumber. The roughness spectral density is related to $f(x)$ by[26]

$$W(K) = \lim_{L\to\infty} \frac{1}{2\pi}\left\langle \frac{1}{L}\left| \int_{-L/2}^{L/2} f(x)e^{-iKx}\,dx \right|^2 \right\rangle, \quad (16)$$

where $\langle\ \rangle$ indicates ensemble averaging.

For the scattering computation, surface realizations (heights and first and second derivatives) are needed at a set of N points with spacing Δx over length $L = N\Delta x$. Realizations with the desired properties can be generated at points $x_n = n\Delta x (n = 1,\ldots,N)$ using

$$f(x_n) = \frac{1}{L}\sum_{j=-N/2}^{N/2-1} F(K_j)e^{iK_j x_n}, \quad (17)$$

where, for $j \geqslant 0$,

$$F(K_j) = [2\pi L W(K_j)]^{1/2} \begin{cases} [N(0,1) + iN(0,1)]/\sqrt{2}, & j \neq 0, N/2, \\ N(0,1), & j = 0, N/2, \end{cases} \quad (18)$$

and, for $j<0$, $F(K_j) = F(K_{-j})^*$. In (18), $K_j = 2\pi j/L$ and each time $N(0,1)$ appears, it indicates an independent sample taken from a zero mean, unit variance Gaussian distribution. Equation (17) is computed with a fast Fourier transform (FFT), as are the first and second derivatives of $f(x)$. In practice, longer realizations of length L' with N' points are first generated and a subset of length L with N points is extracted. Specifically, $N' = 1024$, $N = 400$, and $\Delta x = \lambda/5$; thus $L = 80\lambda$.

For the present work, a Gaussian roughness spectrum is used:

$$W(K) = (lh^2/2\sqrt{\pi})e^{-K^2l^2/4}, \quad (19)$$

where h denotes the rms height and l is the correlation length. The corresponding correlation function is

$$\rho(x) = \int_{-\infty}^{\infty} W(K)e^{iKx}\,dK = h^2 e^{-x^2/l^2}. \quad (20)$$

An example of a surface realization is shown in Fig. 2.

It is instructive to compute the spectral estimates $\hat{W}(K)$ from the surface realizations for comparison with $W(K)$. In continuum notation, instead of (16) we compute

$$\hat{W}(K) = \frac{1}{2\pi L}\left\langle \left| \int_{-L/2}^{L/2} w(x)f(x)e^{-iKx}\,dx \right|^2 \right\rangle, \quad (21)$$

where $w(x)$ is a real non-negative weighting or window function normalized such that

$$\frac{1}{L}\int_{-L/2}^{L/2} w^2(x)dx = 1. \quad (22)$$

The weighting function is chosen to reflect how the surfaces enter into the Monte Carlo scattering computations and so includes the tapering of the incident field. It is not chosen to be optimal for estimating the true spectral density of the random process that generated the surfaces. Correspondence with the scattering computations is made by setting $w^2(x)$ proportional to the energy flux density passing through the mean surface. Thus

$$w^2(x) = e_f(x)/(E_f/L), \quad (23)$$

where $e_f(x)$ is the energy flux density and E_f is the total energy flux; thus E_f/L is the spatially averaged energy flux density on the $z = 0$ plane. With the incident field as given in Sec. I C [apart from a common factor of $\sin\theta/2\rho_0 c$ which cancels in (23); ρ_0 equals the density and c equals the sound speed], we have

$$e_f(x) = \{1 - [1 - 2(1 - 2\cot^2\theta)(x/g)^2]/(kg\sin\theta)^2\} \times e^{-2x^2/g^2},$$
$$\frac{E_f}{L} = \sqrt{\frac{\pi}{2}}\left(\frac{g}{L}\right)\left(1 - \frac{0.5(1 + 2\cot^2\theta)}{(kg\sin\theta)^2}\right). \quad (24)$$

A comparison of $W(K)$ (smooth line) and $\hat{W}(K)$ is shown in Fig. 3. Here, $\hat{W}(K)$ is obtained with 50 surface realizations using the same parameters as in Fig. 2. Reasonable convergence of $\hat{W}(K)$ to $W(K)$ is observed except at low spectral levels. This difference occurs because $w(x)$ still has a small finite value at the surface endpoints, an effect often

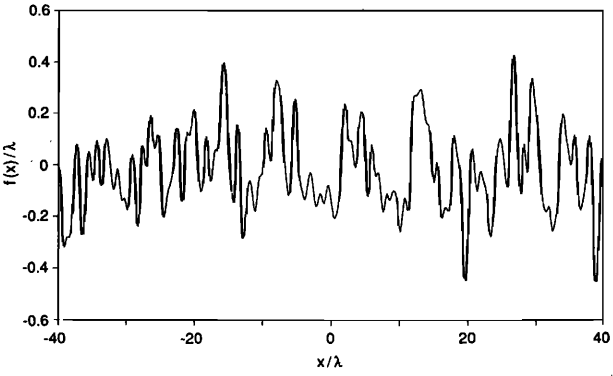

FIG. 2. Surface realization with vertical exaggeration, where $h/\lambda = 0.159$ and $l/\lambda = 0.675$.

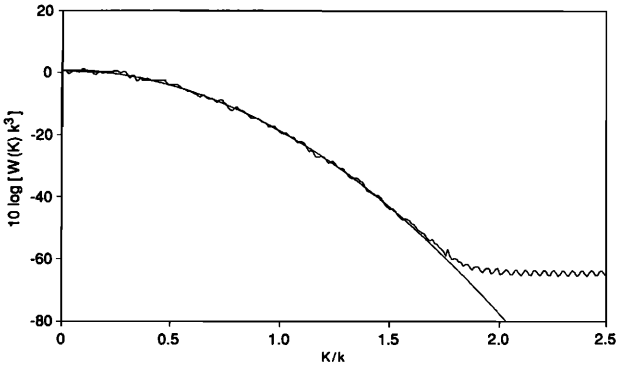

FIG. 3. Comparison of surface spectral density estimate with nominal spectral density (smooth line) for ensemble of 50 surface realizations using surface properties of Fig. 2.

referred to as spectral leakage. The level of the spectral tail could be reduced further by increasing the ratio L/g, but it has an insignificant effect in the present work. If a rectangular window function is used, the level of the spectral tail is 30 dB higher. The corresponding scattering problem with an untapered plane wave (using the numerical method of Sec. I A) does not represent scattering from a Gaussian roughness spectrum. Edge effects dominate the scattered field when the true scattering strength lies below about -30 dB for $L = 80\lambda$.

It has also been useful to compute estimates of the surface rms height, rms slope, and rms second derivative. For example, the estimates for the mean-square height and slope are

$$\hat{h}^2 = \frac{1}{L}\left\langle \int_{-L/2}^{L/2} f^2(x) w^2(x)\, dx \right\rangle ,$$
$$\hat{s}^2 = \frac{1}{L}\left\langle \int_{-L/2}^{L/2} \left(\frac{df}{dx}\right)^2 w^2(x)\, dx \right\rangle . \tag{25}$$

Note that the rms height $\hat{h}$ and rms slope $\hat{s}$ are weighted averages over each surface and over all realizations. For surfaces with Gaussian statistics, the rms height, rms slope, and correlation length are related by[27] $s = \sqrt{2}h/l$, so we obtain an estimate for the correlation length from $\hat{l} = \sqrt{2}\hat{h}/\hat{s}$.

In the following sections, comparisons are made between Monte Carlo Kirchhoff and theoretical Kirchhoff predictions. When $l/\lambda \lesssim 1$, these predictions occasionally differ about 1–2 dB, particularly for bistatic backscattering at relatively low scattered levels, when h and l are used in the theoretical predictions. For parameters used in this work, however, the estimates $\hat{h}$ and $\hat{l}$ may differ up to a few percent from the values of h and l in (19). This indicates that the average properties of the set of surfaces differ slightly from the target values although they are still within expected statistical variations. The difference between the two Kirchhoff calculations disappears when $\hat{h}$ and $\hat{l}$ are used in the theoretical predictions instead of h and l. In the examples that follow in Secs. II and III, no distinction is made between h and l and their estimates but, when there is a difference, the estimates $\hat{h}$ and $\hat{l}$ are used. When $l/\lambda \gtrsim 1$, the relationship between Monte Carlo and theoretical Kirchhoff predictions for bistatic backscattering is somewhat more complicated; this is discussed in Sec. III C.

II. NUMERICAL EXAMPLES

This section introduces the various computations that will be applied to the analysis of the Kirchhoff approximation in Sec. III.

A. First kind versus second kind solutions

Equations (2) and (3) are two formally equivalent integral equations of the first and second kind, respectively, for $\partial p(\bar{r})/\partial n$. Questions have been raised concerning the accuracy of numerical methods based on the integral equation of the first kind.[21] A good discussion of the numerical and mathematical issues is given by Baker.[28] We find that for scattering from 1-D randomly rough surfaces, the equations of the first and second kind give consistent results,[29] so either can be used to obtain the exact solution. A similar conclusion has been reached for the sinusoidal surface,[14,17,30] although in the case of Ref. 17 the agreement was less convincing. The integral equation of the first kind has been used in all of the following examples.

B. Integral equation versus the Kirchhoff approximation: Monte Carlo method

Figure 4 compares the ensemble averaged results over 50 surface realizations for the integral equation and Kirchhoff approximation using a randomly rough surface where the incident grazing angle $\theta = 45°$, $h/\lambda = 0.212$, and $l/\lambda = 0.900$. The rms surface slope $s = \sqrt{2}h/l = 0.333 = \tan\gamma$ so that the rms slope angle $\gamma = 18.4°$. [The Kirchhoff theory curve (smooth line) is discussed in Sec. II C.] The magnitude of the fluctuation in scattering strength with angle is consistent with what is expected for an average over 50 surface realizations and could be reduced by averaging over more surfaces. The integral equation and Kirchhoff approximation results show correlated fluctuations because the same 50 surface realizations are employed in both cases. We see that in this case the integral equation gives lower scattering strengths than the Kirchhoff approximation for scattering angles near 0° and 180° (low scattered grazing angles), but that the two methods are in reasonable agreement over a broad range of scattering angles. Note that direct backscattering occurs at $\theta_s = 45°$ and the Kirchhoff prediction for backscattering is as accurate as it is for scattering near the specular direction ($\theta_s = 135°$).

The specular peak in Fig. 4 is due to the coherent component, which has a finite angular width because of the finite length of the surface. The Rayleigh roughness parameter in the specular direction is $\chi = 2kh \sin\theta = 1.88$ and the coherent reflection loss in the Kirchhoff approximation is $-10\log e^{-\chi^2} = 15.3$ dB. The exact solution indicates a loss of about 2 dB less. The focus in this paper is on the accuracy of the Kirchhoff approximation for the incoherent component.

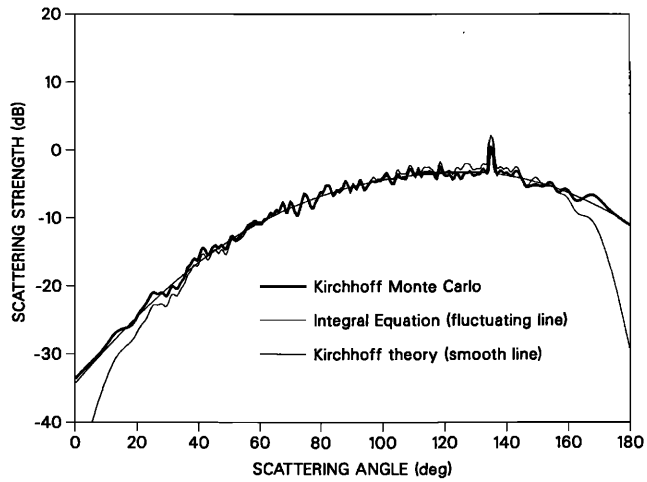

FIG. 4. Scattering strength comparison for $\theta = 45°$, $h/\lambda = 0.212$, $l/\lambda = 0.900$, and $\gamma = 18.4°$. For the integral equation and Kirchhoff Monte Carlo curves, 50 surface realizations were used with $L = 80\lambda$ and $\Delta x = 0.2\lambda$. The integral equation curve has the highest coherent peak.

C. The Kirchhoff approximation with theoretical ensemble averaging

With the Kirchhoff approximation, it is not necessary to use a Monte Carlo method to compute moments of the scattered field. Instead, the statistical properties of the surfaces are used to perform the ensemble average theoretically for the case of a plane wave incident on an arbitrarily long surface. This calculation is now outlined and the results are compared with those of the Monte Carlo method. The scattered coherent field depends explicitly on the surface length if the coherent field is described by a cross section. Thus the standard theoretical method is modified here taking this into account. We compute a "theoretical" total cross section in the Kirchhoff approximation using

$$\sigma_T = \sigma_{\text{incoh}} + R_{\text{coh}} \cdot \sigma_{fs} \,. \tag{26}$$

In (26), σ_{incoh} is the infinite surface length incoherent cross section in the Kirchhoff approximation, which is the 1-D surface analog of the result given, for example, by Ishimaru[31]:

$$\sigma_{\text{incoh}}(\theta,\theta_s) = \left(\frac{k}{2\pi}\right)\left(\frac{1+\sin\theta\sin\theta_s+\cos\theta\cos\theta_s}{\sin\theta+\sin\theta_s}\right)^2 J, \tag{27}$$

where

$$J = \int_{-\infty}^{\infty} dx \cos[kx(\cos\theta+\cos\theta_s)] \times\left(\exp\left[-\chi^2\left[1-\exp\left(\frac{-x^2}{l^2}\right)\right]\right]-\exp(-\chi^2)\right), \tag{28}$$

with $\chi = kh\,(\sin\theta+\sin\theta_s)$. Also, in (26), R_{coh} is the coherent intensity reflection coefficient in the Kirchhoff approximation given by

$$R_{\text{coh}} = e^{-\chi^2} \tag{29}$$

and σ_{fs} is the finite length flat surface cross section in the Kirchhoff approximation. The cross section σ_{fs} is computed numerically using the incident field from Sec. I B; this factor provides a finite angular width for the coherent component.

The two Kirchhoff calculations are compared in Fig. 4. We see that the finite surface length Monte Carlo result is converging well to the theoretical result, which is for an infinite length surface except for the specular peak. It appears that the surfaces are sufficiently long to allow direct comparison between the Monte Carlo output and theory (which is based on infinite length surfaces). In general, however, the most reliable comparisons will be between the exact and approximate methods, which are both applied to the same set of surfaces in Monte Carlo calculations.

We will also find it useful to consider the high-frequency, or geometric optics, limit. The geometric optics cross section is obtained easily from Eqs. (27) and (28) by approximating $1-e^{-x^2/l^2} \cong x^2/l^2$ in (28), which is valid in the high-frequency limit. The result is

$$\sigma_{\text{incoh}} = \frac{1}{2\sqrt{\pi}}\frac{l}{h}\frac{(1+\sin\theta\sin\theta_s+\cos\theta\cos\theta_s)^2}{(\sin\theta+\sin\theta_s)^3} \times\exp\left(-\frac{l^2(\cos\theta+\cos\theta_s)^2}{4h^2(\sin\theta+\sin\theta_s)^2}\right). \tag{30}$$

The exponential factor in Eq. (30) can be written as $\exp(-\tan^2\gamma_0/2s^2)$, where $s=\tan\gamma$ is the rms surface slope and $\gamma_0 = 90° - (\theta_i+\theta_s)/2$. The quantity $-\tan\gamma_0$ is the surface slope necessary to "reflect" a ray from the incident direction to the scattered direction (see Fig. 1). The bistatic scattering cross section in the high-frequency limit is essentially proportional to the probability of occurrence of a surface slope that would reflect a ray from the incident direction to the scattered direction.

D. The shadowing correction

Shadowing occurs in two situations: for low incident grazing angles when sections of the surface are "shadowed" from the incident field and for low scattered grazing angles when sections of the surface lie in shadows with respect to a "receiver." In the latter case, rays cannot be drawn from the surface segments in question to the receiving point without intersecting the surface. The second type of shadowing is clearly related to multiple scattering. Both types are included automatically in the integral equation cross section, while neither is included in the Kirchhoff approximation. Grazing angles can be considered low with regard to shadowing when they are about equal to or are less than the rms slope angle of the surface. For the example in Fig. 4, $\theta = 45°$ and $\gamma = 18.4°$, so only shadowing of the scattered field need be considered. A correction for shadowing in this case will reduce the Kirchhoff prediction at low scattered grazing angles, which is in the direction to reduce the error. In some other cases, particularly for low incident grazing angles, the Kirchhoff approximation yields a significant energy excess in the scattered field which is compensated approximately by the shadowing correction. It is natural then to compare the exact result with the shadow-corrected Kirchhoff prediction to test the accuracy of such a correction. One should bear in mind that shadowing theory is based on high-frequency limit concepts and it is an open question whether it can be applied directly to the Kirchhoff prediction, as is often done in applications. This is certainly an issue in the present example, where $h/\lambda < 1$ and $l/\lambda \sim 1$, while in the high-frequency limit, $h/\lambda \gg 1$ and $l/\lambda \gg 1$.

The shadowing correction developed by Wagner[13] is applied to the "theoretical" Kirchhoff prediction. The form used is from Appendix A in Ref. 13; Wagner showed that it gives excellent agreement with the Monte Carlo shadowing data of Brockelman and Hagfors.[32] In Eq. (26), σ_{incoh} is replaced by $S(\theta,\theta_s)\sigma_{\text{incoh}}$; the shadowing correction factor is given by

$$S(\theta,\theta_s) = \begin{cases} S(\theta_s), & 0 \leqslant \theta_s \leqslant \theta, \\ S(\theta), & \theta \leqslant \theta_s \leqslant 90°, \\ S_1(\theta,\theta_s), & 90° \leqslant \theta_s \leqslant 180°, \end{cases} \tag{31}$$

where

$$S(\theta_s) = [1 + \mathrm{erf}(v_s)](1 - e^{-2B_s})/(4B_s),$$

$$B_s = \{\exp(-9v_s^2/8)/(3\pi v_s^2)^{1/2} + \exp(-v_s^2)/(\pi v_s^2)^{1/2} - [1 - \mathrm{erf}(v_s)]\}/4,$$

$$v_s = |\tan\theta_s|/\sqrt{2}s, \quad s = \text{rms slope} = \sqrt{2}h/l,$$

and

$$S_1(\theta,\theta_s) = [\mathrm{erf}(v) + \mathrm{erf}(v_s)]\{1 - \exp[-2(B + B_s)]\}/[4(B + B_s)].$$

The quantities v, B, and $S(\theta)$ are obtained by substituting θ for θ_s.

The Kirchhoff prediction with and without shadowing is compared in Fig. 5 with the integral equation result from Fig. 4. The shadowing correction does reduce the error, but does not eliminate it for $\theta_s \sim 170°$–$180°$.

One further refinement on the shadowing correction is possible. Because the slope distribution in the "illuminated region" differs from the full slope distribution, the scattering cross section should be modified to account for the change in slope distribution. Using the results obtained by Wagner (Sec. IV of Ref. 13), this additional correction (in the high-frequency limit) can be absorbed into the shadowing correction (31) by replacing $S(\theta_s)$ with $2S(\theta_s)/[1 + \mathrm{erf}(v_s)]$, $S(\theta)$ with $2S(\theta)/[1 + \mathrm{erf}(v)]$, and $S_1(\theta,\theta_s)$ with $2S(\theta,\theta_s)/[\mathrm{erf}(v) + \mathrm{erf}(v_s)]$. These changes always increase $S(\theta,\theta_s)$ at low grazing angles and therefore increase the difference from the integral equation results. It appears that the geometric optics shadowing theory underpredicts the actual shadowing effect for this example, where $l/\lambda \sim 1$. This will be discussed further in Sec. III.

III. ANALYSIS OF THE KIRCHHOFF APPROXIMATION

The validity criterion commonly used for the Kirchhoff approximation is based on the local radius of curvature of the surface. For a deterministic surface, the criterion is that at each point on the surface[33]

$$2k|R|\sin^3\theta_g \gg 1, \tag{32}$$

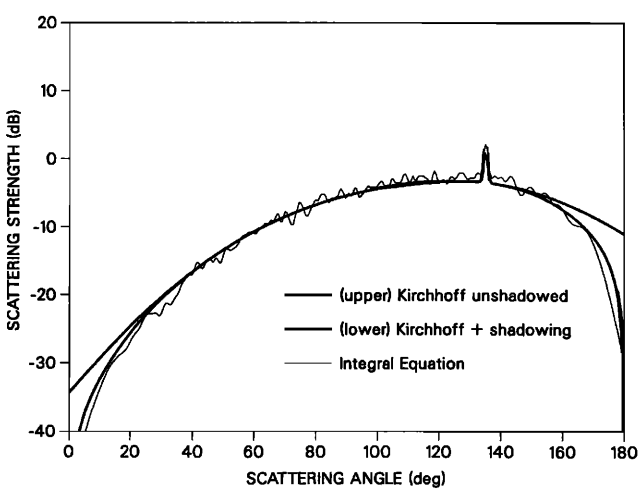

FIG. 5. The unshadowed and shadow-corrected Kirchhoff prediction with the integral equation result from Fig. 4.

where k is the acoustic wavenumber, R is the radius of curvature, and θ_g is the local grazing angle of the incident field (Fig. 1). A corresponding criterion for randomly rough surfaces can be written as

$$2k\tilde{R}\sin^3\theta \gg 1, \tag{33}$$

where $\tilde{R}$ denotes an "rms radius of curvature" and θ is the grazing angle with respect to the plane of the mean surface. For a deterministic surface $f(x)$, the (signed) radius of curvature is given by

$$R = \left[1 + \left(\frac{df}{dx}\right)^2\right]^{3/2} \Big/ \frac{d^2f}{dx^2}. \tag{34}$$

For a random surface, we use the following estimator[34] for the average radius of curvature:

$$\tilde{R} = \left[1 + \left\langle\left(\frac{df}{dx}\right)^2\right\rangle\right]^{3/2} \Big/ \left\langle\left(\frac{d^2f}{dx^2}\right)^2\right\rangle^{1/2}, \tag{35}$$

which, for a Gaussian roughness spectrum, becomes

$$\tilde{R} = (l^2/\sqrt{12}h)(1 + 2h^2/l^2)^{3/2}. \tag{36}$$

With the Gaussian roughness spectrum (19), the parameter space of interest involves h/λ, l/λ, θ, and θ_s. A logical goal is to replace (33) with a condition involving these parameters that guarantees accuracy of the Kirchhoff prediction to within a given limit—for example, 2 dB. This approach has not proved to be practical. As a starting point, in two respects (33) turns out to be deficient as it stands. First, both the Kirchhoff approximation [e.g., see Eq. (27)] and the exact scattering cross sections satisfy reciprocity—that is, the scattering cross section $\sigma(\theta,\theta_s)$ is invariant to the interchange of θ and θ_s as defined in Fig. 1. It follows that any criterion should also satisfy reciprocity; (33) clearly does not. Second, as will be seen later, $\tilde{R}$ is not the key surface parameter for delimiting the region of validity of the Kirchhoff approximation, nor has some other simple inequality involving h/λ, l/λ, θ, and θ_s emerged to replace (33). Instead, a more indirect strategy has been adopted to define the validity region, as will be discussed later.

A. Examples of error in the Kirchhoff approximation

We begin by briefly reviewing the example in Sec. II. For this case, the "Kirchhoff parameter" $2k\tilde{R}\sin^3\theta = 5.74$, so (33) is reasonably satisfied. Also, $\theta = 45°$, which is more than twice the rms slope angle of 18.4°. In Fig. 4, the Kirchhoff approximation gives accurate scattering strengths over a broad range of scattering angles, but it predicts high values at low scattered grazing angles (θ_s near 0° or 180°). The application of Wagner's[13] shadowing correction in Fig. 5 improves the agreement with the integral equation. However, the result could be interpreted to mean the actual shadowing effect is greater than that given by Wagner's[13] correction for this case, where $l/\lambda \sim 1$. The enhancement over geometric optics shadowing persists to larger values of l/λ, as will be discussed later.

Figure 6 illustrates the behavior at a shorter correlation length. Again, $\theta = 45°$ and $\gamma = 18.4°$, but both h/λ and l/λ have been reduced by a factor of 2 from the values used for Figs. 4 and 5 to $h/\lambda = 0.106$ and $l/\lambda = 0.450$. Here, the Kirchhoff parameter is $2k\tilde{R}\sin^3\theta = 2.87$, so (33) may not

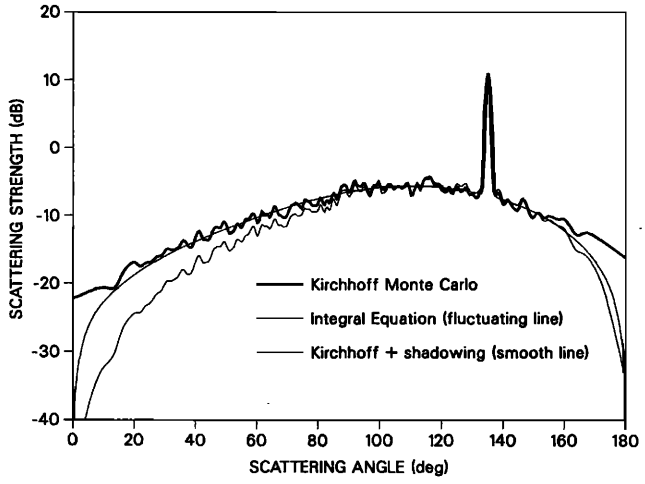

FIG. 6. Effect of reduced correlation length: $\theta = 45°$, $h/\lambda = 0.106$, $l/\lambda = 0.450$, and $\gamma = 18.4°$.

be satisfied. We observe a more general breakdown of the Kirchhoff approximation for bistatic backscattering, although it remains accurate near the specular direction. The much larger specular peak occurs here because the reduced Rayleigh roughness parameter ($2kh \sin\theta = 0.94$) leads to a coherent reflection loss of only 3.9 dB in the Kirchhoff approximation. Evidently, shadowing is not related to the Kirchhoff integral equation differences for θ_s between 30° and 80°; instead, a new and more fundamental source of error appears for the Kirchhoff approximation as l/λ is reduced below ~ 1.

Finally, Fig. 7 shows the effect of increasing the average radius of curvature while holding the correlation length at the value for Fig. 6. The radius of curvature has been increased by reducing h/λ by a factor of 2 to $h/\lambda = 0.053$ [see Eq. (36)]. With $l/\lambda = 0.450$, the rms slope angle becomes 9.5° and the Kirchhoff parameter is $2k\tilde{R}\sin^3\theta = 5.11$, close to its value of 5.74 in Figs. 4 and 5. However, Figs. 6 and 7 show very similar behavior: The Kirchhoff approximation yields significantly high scattering strengths over a broad range of scattering angles for bistatic backscattering.

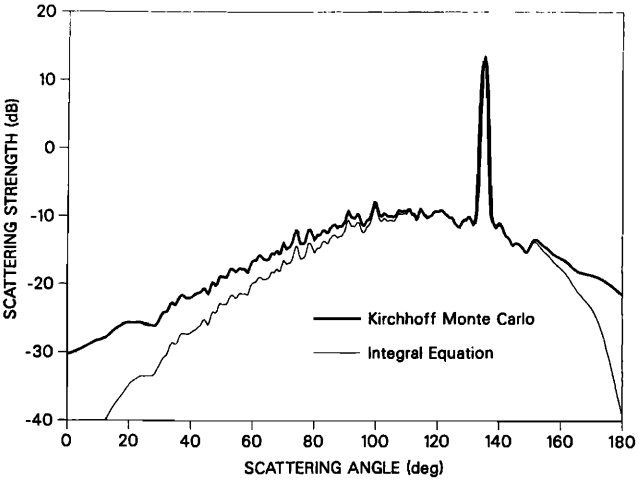

FIG. 7. Radius of curvature increased a factor of ~ 1.8 relative to Fig. 6: $\theta = 45°$, $h/\lambda = 0.053$, $l/\lambda = 0.450$, and $\gamma = 9.5°$.

Consistent results have been obtained in all examples investigated. As l/λ is reduced below ~ 1, the Kirchhoff prediction becomes high, as in Figs. 6 and 7. The magnitude of the error is closely correlated with l/λ and not with $\tilde{R}/\lambda$ or the Kirchhoff parameter. For example, in Figs. 4 and 5, $\tilde{R}/\lambda = 1.292$; in Fig. 6, $\tilde{R}/\lambda = 0.646$; and in Fig. 7, $\tilde{R}/\lambda = 1.149$. Yet the Kirchhoff approximation gives similar error in Figs. 6 and 7, where $l/\lambda = 0.450$, and much less error in Figs. 4 and 5, where $l/\lambda = 0.900$. We find that the particular combination of h and l that enters into the radius of curvature is not closely related to the Kirchhoff error; rather, the correlation length alone is the key parameter for assessing the magnitude of the error away from the low grazing angle region.

B. Comparison with first-order perturbation theory

Before pursuing the characterization of the Kirchhoff approximation error, a comparison with first-order perturbation theory is of interest. In Figs. 6 and 7, h/λ is 0.106 and 0.053, respectively. One might suppose that at such low values of rms surface height, the region of applicability of first-order perturbation theory has been reached, making the accuracy of the Kirchhoff approximation less important. In first-order perturbation theory, the incoherent scattering cross section is given by

$$\sigma = 4k^3 \sin^2\theta \sin^2\theta_s \, W[k(\cos\theta + \cos\theta_s)], \quad (37)$$

with the surface roughness spectral density $W(K)$ given by (19). Equation (37) is the 1-D surface analog of the 2-D surface result given, for example, by Ishimaru.[31,35]

The first-order perturbation theory prediction for the cases of Figs. 6 and 7 are compared with the integral equation results in Fig. 8. In the first-order perturbation curves, the coherent component has not been included; hence, the specular peak is missing. For $h/\lambda = 0.106$ [Fig. 8(a)], first-order perturbation theory is clearly not a good approximation, while even for $h/\lambda = 0.053$ [Fig. 8(b)], agreement is only good for $\theta_s \gtrsim 60°$.

A detailed investigation of the valid region of first-order perturbation theory will be given elsewhere. Here, we merely note that, for the example given by Fig. 6, neither the Kirchhoff approximation nor first-order perturbation theory is accurate for bistatic backscattering. Notice that for $\theta_s \cong 170°$–180°, first-order perturbation theory is accurate. As expected, shadowing corrections to first-order perturbation theory are unnecessary. The drop in the scattering strength as $\theta_s \to 180°$ in Fig. 8 enters the first-order perturbation result through an interference effect and is not associated readily with geometric shadowing concepts. However, the Kirchhoff result in this region (Fig. 6) has not reduced down to the first-order perturbation theory result and a shadowing correction is needed.

C. Error in the shadowing correction

Figure 9 shows the forward scattering region for examples with $l/\lambda = 1.50$ and $l/\lambda = 3.00$. These can be compared with Fig. 5, where $l/\lambda = 0.90$. For all three cases, $\theta = 45°$ and $\gamma = 18.4°$. As l/λ increases, the accuracy of the shadowing correction extends to lower grazing angles (θ_s closer to

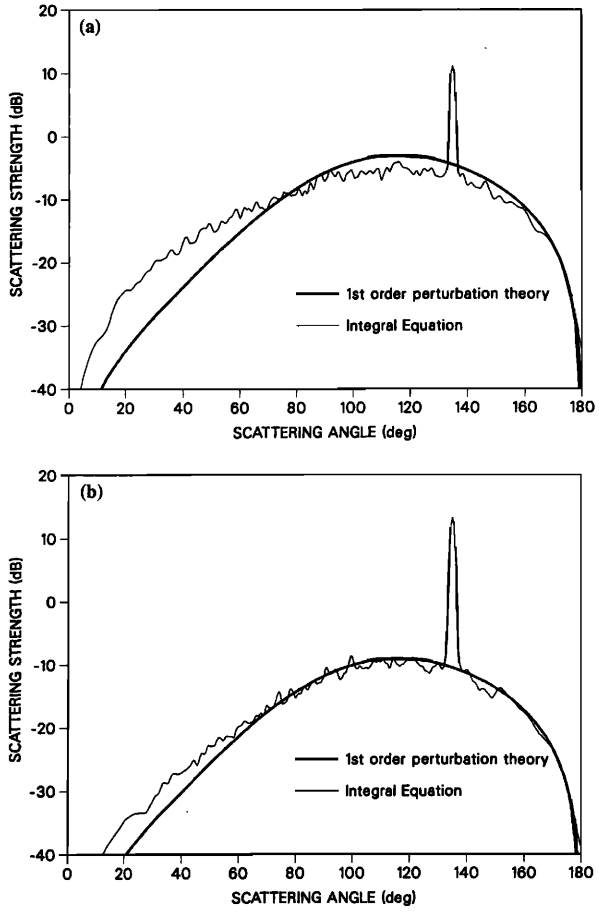

FIG. 8. First-order perturbation prediction (excluding coherent component) compared with integral equation results from (a) Fig. 6 and (b) Fig. 7.

180°). When the shadowing correction has significant error, the integral equation result lies below the shadow-corrected Kirchhoff result. Thus the actual shadowing effect is greater than predicted by theory based on geometric optics.

As a check on possible surface length dependence when the correlation length is relatively long, the example in Fig. 9(b) is redone with double the surface length ($L = 160\lambda$, $N = 800$) in Fig. 10.

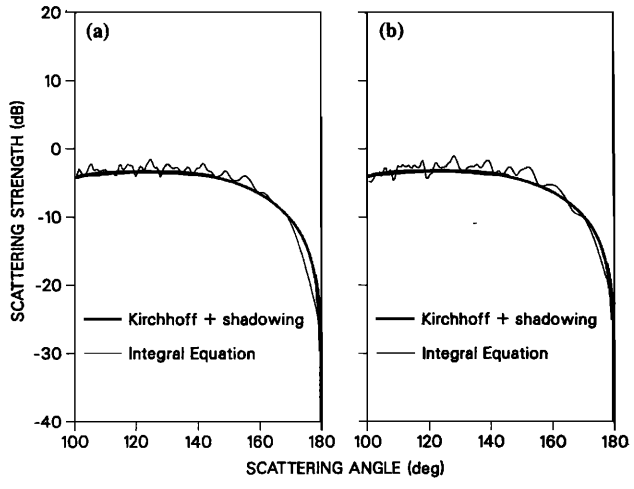

FIG. 9. Accuracy of shadowing correction at longer correlation lengths: $\theta = 45°$, $\gamma = 18.4°$, (a) $h/\lambda = 0.353$, $l/\lambda = 1.50$; (b) $h/\lambda = 0.701$, $l/\lambda = 3.00$.

Figure 10(a) shows that the error in the shadowing correction ($\theta_s = 170°$–$180°$) is not changed significantly. The error may appear small in Fig. 10(a), just below $\theta_s = 180°$, but it reaches 3 dB before the finite angular resolution of the integral equation scattering strength becomes a factor as θ_s approaches 180° (angular resolution is discussed briefly in the Appendix). Figure 10(b) illustrates the exceptional accuracy of the Kirchhoff approximation for backscattering for surfaces with long correlation lengths.

Figure 10(c) shows an effect alluded to at the end of Sec. I E: differences in the Kirchhoff Monte Carlo and Kirchhoff theoretical calculations for bistatic backscattering when $l/\lambda \gtrsim 1$. A corresponding effect is apparent in Fig. 10(a). As l/λ and h/λ increase, the Kirchhoff prediction approaches the geometric optics result of Eq. (30), as shown in Fig. 10(d). In this limit, the scattering cross section is proportional to the probability of occurrence of a surface slope that will "reflect" a ray from the incident to the scattered direction. Relatively high slopes are required for backscattering and the probability of occurrence can become extremely small, thereby leading to large fluctuations in scattering level. Detailed investigation of the surface slopes for the case of Fig. 10 shows a deficiency in the appropriate slopes corresponding to $\theta_s < 40°$, the same region where the discrepancies appear in Fig. 10(a) and (c). Similar behavior is observed for other examples with $l/\lambda \gtrsim 1$. Presumably, larger ensemble sizes would improve agreement in this region, although the slope probabilities can become so low that this approach is impractical for Monte Carlo work. This example illustrates that the most reliable comparisons are made between exact and approximate methods when both are applied to the same set of surfaces in Monte Carlo calculations.

As one further aside from the shadowing discussion, there is a tendency in Figs. 5, 9, and 10 for the integral equation scattering strengths to be up to 1 dB higher than the shadowed Kirchhoff scattering strengths for $120° \lesssim \theta_s \lesssim 160°$. This error is not considered significant, but may become so if the condition $\theta \gtrsim 2\gamma$ is not maintained. This point will be discussed in Sec. III E.

We now return to the consideration of shadowing. The magnitude of the Wagner[13] shadowing correction is about 1 dB when $|\tan\theta_s| \cong \tan\gamma = s$, where s is the rms surface slope. This is consistent with Figs. 5, 9, and 10. However, at shorter correlation lengths, the needed shadowing correction becomes greater and appears independent of the rms surface slope (compare Fig. 6, where $\gamma = 18.4°$ with Fig. 7, where $\gamma = 9.5°$). If we are to extend shadowing concepts into the regime of Figs. 6 and 7, a significant change is required in geometric optics shadowing theory.

A simple modification to shadowing theory has been found which replicates the integral equation results reasonably well down to $l/\lambda = 0.45$, the shortest correlation length studied. The procedure is to use an effective surface slope s' given by

$$s' = \max\begin{cases} 1/\sqrt{kl}, \\ s, \end{cases} \tag{38}$$

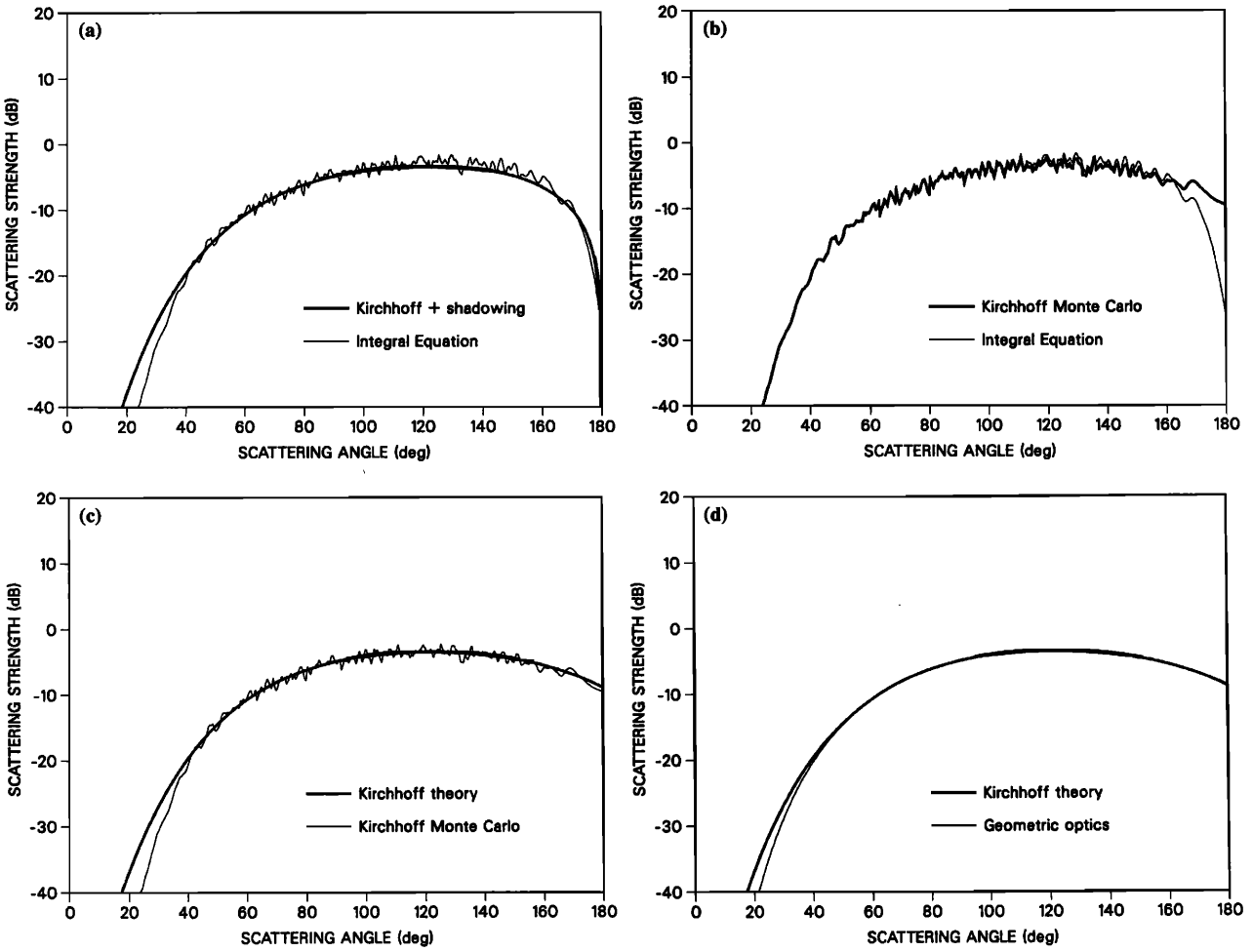

FIG. 10. Same parameters as Fig. 9(b), but with double the surface length for integral equation and Kirchhoff Monte Carlo calculations.

in the shadowing computation. When $s > 1/\sqrt{kl}$, as it is for Figs. 9 and 10, the algorithm reduces to Wagner[13] shadowing. When $s < 1/\sqrt{kl}$, the modified shadowing algorithm becomes independent of surface slope, as implied by Figs. 6 and 7. The result of using (38) when $s < 1/\sqrt{kl}$ is shown in Sec. III D, where short correlation length cases are considered. We also find that, for $s > 1/\sqrt{kl}$, the Wagner[13] shadowing correction is accurate for scattering angles given approximately by

$$|\tan \theta_s| \gtrsim 1/2\sqrt{kl} \ . \tag{39}$$

Equation (39) implies that shadowing theory should be valid down to a grazing angle of about 9.2° in Fig. 9(a) and 6.6° in Figs. 9(b) and 10(a). In the forward direction, the difference between the integral equation and shadowed Kirchhoff results reaches 1 dB at grazing angles of 9.1° in Fig. 9(a), 7.1° in Fig. 9(b), and 6.0° in Fig. 10(a). Similar results are found in other examples, although the difference between the angle given by Eq. (39) and the 1-dB point occasionally exceeds 1°.

Some motivation for rules (38) and (39) is suggested by an analogy with Fresnel diffraction by the edge of an opaque screen. This is discussed in Ref. 30.

D. Effective correlation length

We now turn to a discussion of the Kirchhoff approximation error at short correlation lengths (Figs. 6 and 7). As noted previously, the error increases for bistatic backscattering as l/λ is reduced below 1. Inspection of numerous results does not suggest an analytic inequality that describes accurately the validity region in the parameter space of interest. Instead we have found that the integral equation predictions can be replicated by using an effective correlation length $l' > l$ in the theoretical Kirchhoff calculations. At present, this replacement is not based on theory, yet it does appear to be an important organizing principle for interpreting the results.

Figure 11 shows l'/λ as a function of l/λ obtained from a series of runs holding θ and γ constant at 45° and 18.4°, respectively. The appropriate l' was obtained to yield the best fit to the integral equation scattering strength in each case. The shadowing correction described by Eq. (38) was used. The difference $\Delta l/\lambda = (l' - l)/\lambda$ is well approximated by

$$\Delta l/\lambda = -0.144 l/\lambda + 0.150 \tag{40}$$

for $0.45 < l/\lambda < 1.04$.

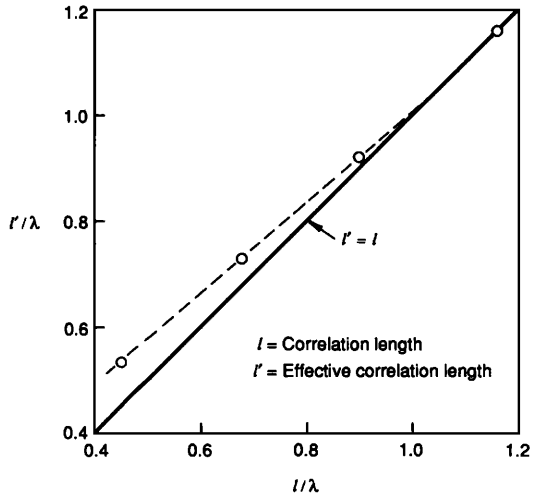

FIG. 11. Effective correlation length (circles) found to yield good agreement with integral equation results when used in Kirchhoff calculation (modified Kirchhoff): $\theta = 45°$ and $\gamma = 18.4°$. The size of the circle indicates the uncertainty in l'/λ.

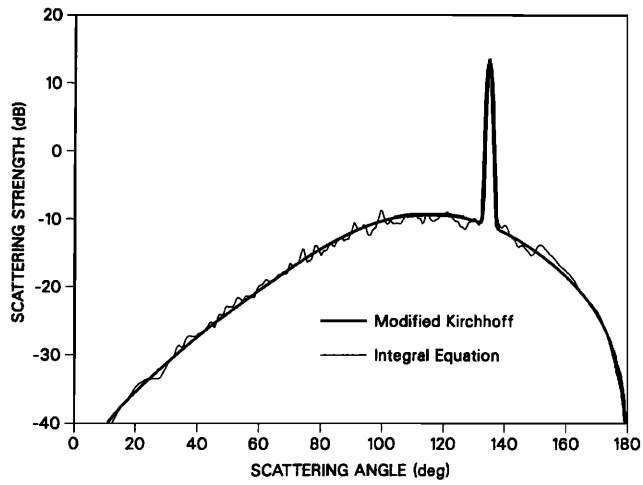

FIG. 13. Modified Kirchhoff calculation compared with integral equation result from Fig. 7: $\theta = 45°$, $h/\lambda = 0.053$, $l/\lambda = 0.450$, and $\gamma = 9.5°$.

The case for $l/\lambda = 0.45$ in Fig. 11 is the same as shown originally in Fig. 6; the result of the modified Kirchhoff calculation is shown in Fig. 12. Increasing l/λ to $l'/\lambda = l/\lambda + 0.085$ and using the shadowing correction that follows from Eq. (38) yield excellent agreement with the integral equation method. This procedure might be considered to be just numerology except that, once l'/λ is found, it works equally well in other examples as long as the original correlation length is the same. The example in Fig. 7 was also for $l/\lambda = 0.45$ and $\theta = 45°$, but h/λ was reduced so that $\gamma = 9.5°$ instead of 18.4°. The result with the same l'/λ as used in Fig. 12 is given in Fig. 13; again, the agreement is excellent. The change in correlation length causes little difference in the scattering strengths to the right of the specular peak; the agreement in that region arises from the shadowing correction with $s' = 1/\sqrt{kl}$.

Similar results have been obtained at the other l/λ values in Fig. 11 and at incident grazing angles from 90° down to 20°. However, at low incident grazing angles (including 20°), new effects enter the picture for forward scattering. Aside from this exception, which is discussed in Sec. III E, the modified Kirchhoff calculation outlined here coincides to within about 1 dB of the integral equation prediction over a significant range of parameters. For a Gaussian roughness spectrum, we may assess the accuracy of the shadow-corrected Kirchhoff approximation by comparing the standard and modified predictions: When they diverge, the standard prediction can be assumed to be in error. Also, the difference in scattering strengths between the two methods will give an accurate estimate of the error if the difference is less than 5 dB. This procedure cannot be assumed to apply directly to other roughness spectra and further work is needed to evaluate the Kirchhoff approximation for such cases.

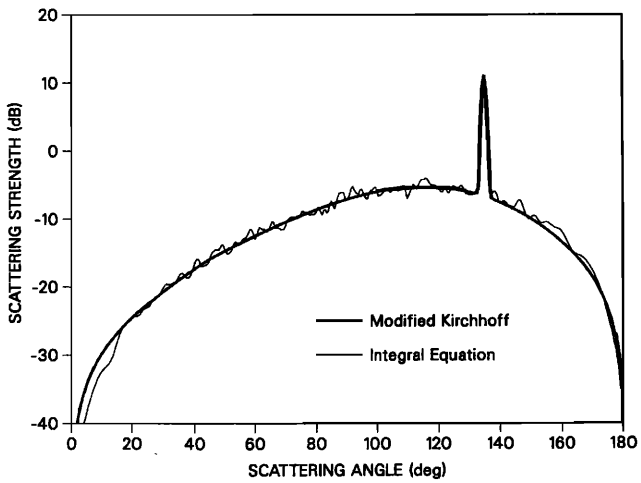

FIG. 12. Modified Kirchhoff calculation compared with integral equation result from Fig. 6: $\theta = 45°$, $h/\lambda = 0.106$, $l/\lambda = 0.450$, and $\gamma = 18.4°$.

E. Low incident grazing angles

New features appear as θ is reduced to less than 2γ. An example with $\theta = 20°$, $\gamma = 18.4°$, and $l/\lambda = 1.19$ is shown in Fig. 14. A nearly constant offset between the integral equation and Monte Carlo Kirchhoff scattering strengths can be noted for $\theta_s \lesssim 120°$. This difference arises from shadowing of the incident field. Near the specular direction ($\theta_s = 160°$), however, the Kirchhoff approximation is accurate. The shadow-corrected theoretical result agrees reasonably well with the integral equation for $\theta_s \lesssim 140°$. (Because $l/\lambda > 1$, no correlation length correction is needed here.) The shadowing correction actually introduces error for $140° \lesssim \theta_s \lesssim 175°$. Even greater error is found at shorter correlation lengths with θ and γ held constant.

Incidentally, examples at low incident grazing angles such as Fig. 14 make it clear that shadowing of the coherent field is inappropriate; the exact result has an enhanced coherent component in comparison to the unshadowed Kirchhoff result. Wagner[13] suggests doubling the shadowing correction for the coherent field, but (as mentioned in Sec. II D) the shadowing correction is applied only to the incoherent cross section.

There appear to be two new features associated with incoherent forward scattering in Fig. 14. First, for these pa-

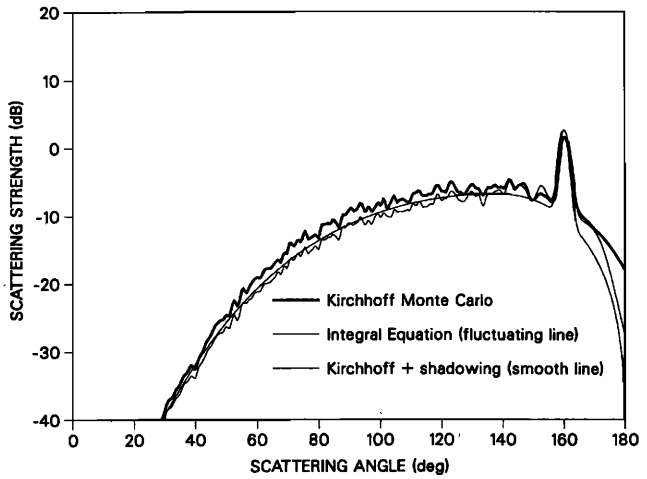

FIG. 14. An example with $\theta \cong \gamma$ and incident field shadowing: $\theta = 20°$, $h/\lambda = 0.280$, $l/\lambda = 1.188$, and $\gamma = 18.4°$. The integral equation curve has the highest coherent peak. For $\theta_s > 160°$, the integral equation curve lies above the shadowed Kirchhoff result.

rameters, the Kirchhoff cross section is approaching the first-order perturbation cross section, so the appropriateness of applying any shadowing correction at all is questionable. Second, allowing θ to drop below $\sim 2\gamma$ appears to enhance the multiple scattering contribution to the cross section near the specular direction in a way that is not taken into account with the shadowing correction.

The shadowing correction becomes too great well before the Kirchhoff cross section reduces to the first-order perturbation cross section. We have found that a convenient way of inferring that shadowing is becoming inappropriate is to compare the Kirchhoff and geometric optics predictions; this is done in Fig. 15 for the parameters used in Fig. 14. Diffraction yields higher backscattering levels ($\theta_s < 80°$) for the Kirchhoff approximation, as expected. Numerical experience indicates that when the Kirchhoff cross section drops significantly below the geometric optics cross section in the forward direction, as it does in Fig. 15 for $\theta_s \gtrsim 160°$, standard shadowing corrections are inappropriate. Evidently, this cross section rolloff as $\theta_s \to 180°$ occurs because of an interference effect among neighboring scattering sites on the rough surface; thus shadowing concepts no longer apply. If shadowing is applied here, the shadowed cross section will be too low (Fig. 14).

Using the "Kirchhoff geometric optics comparison test," the examples in Figs. 12 and 13 are found to be marginal for shadowing corrections in the forward direction (in fact, the case in Fig. 12 does not appear to pass the test). This probably accounts (fortuitously) for the very good agreement obtained for $\theta_s > 160°$ in these two examples when using the shadowing correction. The tendency for the shadowing correction to be too small for $|\tan \theta_s| \lesssim 1/(2\sqrt{kl})$ is apparently balanced by the tendency for the shadowing correction to be too large when the Kirchhoff cross section drops significantly below the geometric optics cross section.

Two final examples are given in Figs. 16 and 17, where $\theta = 20°$. In each case, l and h have been increased so that the Kirchhoff cross sections do not drop much below the geometric optics cross sections, as shown in Figs. 16(a) and 17(a). In Fig. 16, $\gamma = 10.1°$, so $\theta/\gamma \cong 2$. The shadow-corrected Kirchhoff approximation has acceptable error consistent with Eq. (39). In Fig. 17, $\gamma = 18.4°$ and the shadow-corrected Kirchhoff approximation shows noticeable error, especially near the specular direction. Consistent results are obtained when the surface length is doubled ($L = 160\lambda$, $N = 800$). Our presumption is that, when $\theta/\gamma \lesssim 2$, a significant amount of scattered energy is redistributed to higher scattered grazing angles by multiple scattering, causing the error in Fig. 17(b).

It appears that an assessment of Kirchhoff validity at low grazing angles ($\theta \lesssim 2\gamma$) for forward scattering is made difficult by multiple scattering effects that cannot be simply described with shadowing corrections. Comparisons with multiple scattering theory will probably be necessary to fully understand this region.

IV. SUMMARY

The validity of the Kirchhoff approximation applied to scattering from 1-D surfaces with a Gaussian roughness

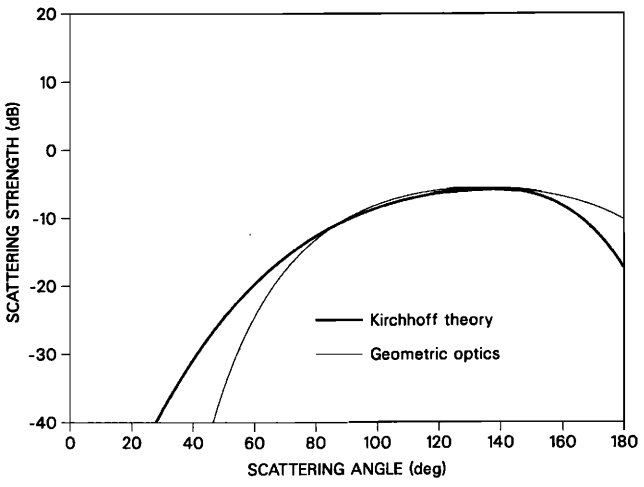

FIG. 15. Comparison of Kirchhoff (coherent component excluded) and geometric optics predictions for the example in Fig. 14.

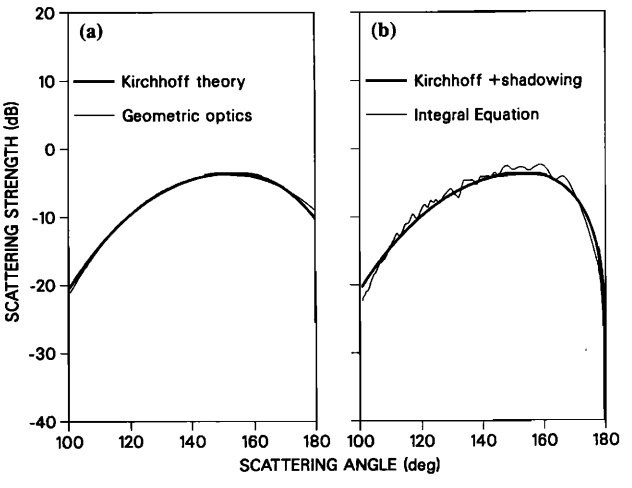

FIG. 16. Example where the shadow-corrected Kirchhoff prediction is accurate, where $\theta/\gamma \cong 2$: $\theta = 20°$, $h/\lambda = 0.60$, $l/\lambda = 4.75$, and $\gamma = 10.1°$.

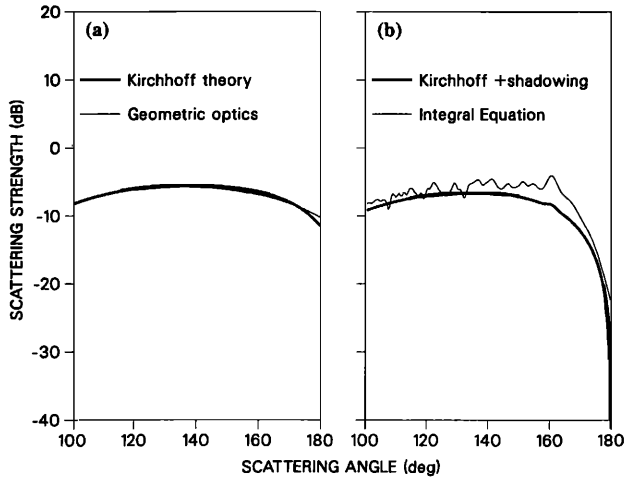

FIG. 17. Example where the shadow-corrected Kirchhoff prediction is not accurate, where $\theta/\gamma \cong 1.1$: $\theta = 20°$, $h/\lambda = 0.56$, $l/\lambda = 2.38$, and $\gamma = 18.4°$.

spectrum has been examined by comparison with exact integral equation results. The surface correlation length l, rather than the rms radius of curvature, is found to be the important parameter in defining the region of Kirchhoff validity away from the low grazing angle region. At low grazing angles, additional dependence enters through the rms slope $s = \tan\gamma = \sqrt{2}h/l$, or through an effective rms slope $s' = 1/\sqrt{kl}$.

Examples are considered first where the incident grazing angle θ is $\gtrsim 2\gamma$; throughout, the rms slope angle γ is restricted to $\lesssim 20°$. When $l/\lambda \gtrsim 1$, the Kirchhoff approximation is accurate, except at low scattered grazing angles where $|\tan\theta_s| \lesssim \tan\gamma$. For these cases, the shadowing correction developed by Wagner[13] is found to be accurate down to lower scattered grazing angles such that $|\tan\theta_s| \lesssim 1/(2\sqrt{kl})$.

When $l/\lambda \lesssim 1$, the Kirchhoff approximation predicts high scattering strengths for bistatic backscattering. The correct scattering levels are replicated using an effective correlation length $l' > l$ (Fig. 11) in the theoretical Kirchhoff calculation. The appropriate effective correlation length appears to depend only on the actual correlation length and not on the rms surface slope (for $\gamma \lesssim 20°$) nor on the incident grazing angle. Also, at short correlation lengths such that $1/\sqrt{kl} > s$, where s is the rms surface slope, the apparent shadowing effect is greater than given by Wagner's[13] correction. Use of an effective slope $s' = 1/\sqrt{kl}$ for the shadowing correction when $s' > s$ replicates the integral equation results. This is a simple method for approximately accounting for diffractive multiple scattering effects. These prescriptions for an effective correlation length and surface slope can be used for a quantitative determination of the accuracy of the Kirchhoff approximation (Secs. III C and D).

When $\theta \lesssim 2\gamma$, the Kirchhoff accuracy can still be assessed for bistatic backscattering using the method described, but forward scattering becomes more complicated (Sec. III E). In this region, multiple scattering evidently enhances the cross section near the specular direction; therefore, shadowing corrections are no longer sufficient to handle the effects of multiple scattering. Finally, we find examples at low incident grazing angles (and low Rayleigh roughness parameters) where the concept of shadowing breaks down; for these cases, the shadowing correction increases the error. Here, the Kirchhoff result is approaching the first-order perturbation theory result where shadowing is not appropriate. Further work is required to fully understand the applicability of the Kirchhoff approximation to forward scattering with low incident grazing angles.

ACKNOWLEDGMENTS

This work was supported by the Office of Naval Research, Code 1125OA. Some of the computing was done at the San Diego Supercomputer Center, whose support is appreciated. Programming was done by Kate Bader, and Bradley Bell assisted with generation of random surfaces. I wish to thank Darrell Jackson, Dale Winebrenner, and Shira Lynn Broschat for helpful comments.

APPENDIX

Equation (11) in Sec. I B gives an incident field that satisfies the wave equation to order $1/(kg\sin\theta)^2$, where $kg\sin\theta \gg 1$. An incident field constructed from an angular spectrum of plane waves will be an exact solution to the wave equation. One such form is given by

$$p_{\text{inc}}(\bar{r}) = \frac{1}{\sqrt{\pi}\Delta\theta}\int_0^{\pi} \exp\left(\frac{-(\theta'-\theta)^2}{(\Delta\theta)^2}\right) \times \exp(i\bar{k}'\cdot\bar{r})\,d\theta', \tag{A1}$$

with θ equal to the mean grazing angle and $\Delta\theta = 2/(kg\sin\theta)$. Here, g is a parameter controlling the tapering of the incident field. A corresponding expression for $\partial p_{\text{inc}}(\bar{r})/\partial n$ follows readily from Eq. (A1).

Equation (11) can be obtained as an approximation to Eq. (A1) with the following sequence of steps. Let $\delta = \theta' - \theta$ and expand $\bar{k}'\cdot\bar{r} = k[\cos(\theta+\delta)x + \sin(\theta+\delta)z]$ in δ, retaining terms up to δ^2. Then, transforming the integration variable to δ and extending the limits to $\pm\infty$ yield Eq. (11) after integration and some rearrangement, valid to order $1/(kg\sin\theta)^2$. As noted previously, comparisons of first and second kind integral equation solutions using (A1) and (11) show (11) to be entirely adequate.

The angular width of the incident field implied by (A1) [and hence by (11)] is approximately $\sqrt{\pi/2}\Delta\theta$. Therefore, with $g/\lambda = 20$, the computed scattering strengths can be considered averages over about $\pm 0.8°$ for $\theta = 45°$ and about $\pm 1.7°$ for $\theta = 20°$.

Similarly, the angular resolution of the scattered field will be inversely proportional to both the surface length and $\sin\theta_s$. Effects of the finite angular resolution become noticeable if the scattering strength drops rapidly as $\sin\theta_s \to 0$. In such cases an upward bias in the scattering strengths is observed for scattered grazing angles below about 5° [compare Figs. 9(b) and 10(a)].

[1]S. O. Rice, "Reflections of electromagnetic waves from slightly rough surfaces," Comm. Pure Appl. Math. **4**, 351–378 (1951).
[2]E. Y. Harper and F. M. Labianca, "Perturbation theory for scattering of sound from a point source by a moving rough surface in the presence of refraction," J. Acoust. Soc. Am. **57**, 1044–1051 (1975).
[3]C. Eckart, "The scattering of sound from the sea surface," J. Acoust. Soc. Am. **25**, 566–570 (1953).
[4]F. G. Bass and I. M. Fuks, *Wave Scattering from Statistically Rough Surfaces* (Pergamon, Oxford, 1979), Chap. 7.
[5]E. Y. Harper and F. M. Labianca, "Scattering of sound from a point source by a rough surface progressing over an isovelocity ocean," J. Acoust. Soc. Am. **58**, 349–364 (1975).
[6]J. F. McDonald and R. C. Spindel, "Implications of Fresnel corrections in a non-Gaussian surface scatter channel," J. Acoust. Soc. Am. **50**, 746–757 (1971).
[7]J. F. McDonald and P. M. Schultheiss, "Asymptotic frequency spread in surface-scatter channels over an isovelocity ocean," J. Acoust. Soc. Am. **57**, 160–164 (1975).
[8]The term "bistatic" implies that incident and scattered angles differ.
[9]R. R. Lentz, "A numerical study of electromagnetic scattering from ocean-like surfaces," Radio Sci. **9**, 1139–1146 (1974).
[10]R. M. Axline and A. K. Fung, "Numerical computation of scattering from a perfectly conducting random surface," IEEE Trans. Antennas Propag. **AP-26**, 482–488 (1978); corrections to "Numerical computation of scattering from a perfectly conducting random surface," IEEE Trans. Antennas Propag. **AP-28**, 949 (1980).
[11]S. T. McDaniel and A. D. Gorman, "An examination of the composite-roughness scattering model," J. Acoust. Soc. Am. **73**, 1476–1486 (1983).
[12]D. R. Jackson, D. P. Winebrenner, and A. Ishimaru, "Application of the composite roughness model to high-frequency bottom backscattering," J. Acoust. Soc. Am. **79**, 1410–1422 (1986).
[13]R. J. Wagner, "Shadowing of randomly rough surfaces," J. Acoust. Soc. Am. **41**, 138–147 (1966).
[14]P. M. van den Berg, "Diffraction theory of a reflection grating," Appl. Sci. Res. **24**, 261–293 (1971).
[15]K. A. Zaki and A. R. Neureuther, "Scattering from a perfectly conducting surface with a sinusoidal height profile: TE polarization," IEEE Trans. Antennas Propag. **AP-19**, 208–214 (1971).
[16]S. Chuang and J. A. Kong, "Scattering of waves from periodic surfaces," Proc. IEEE **69**, 1132–1144 (1981).
[17]D. F. McCammon and S. T. McDaniel, "Application of a new theoretical treatment to an old problem; sinusoidal pressure release boundary scattering," J. Acoust. Soc. Am. **78**, 149–156 (1985).
[18]D. F. McCammon and S. T. McDaniel, "Surface velocity, shadowing, multiple scattering, and curvature on a sinusoid," J. Acoust. Soc. Am. **79**, 1778–1785 (1986).
[19]H. L. Chan and A. K. Fung, "A numerical study of the Kirchhoff approximation in horizontally polarized backscattering from a random surface," Radio Sci. **13**, 811–818 (1978).
[20]A. K. Fung and M. F. Chen, "Numerical simulation of scattering from simple and composite random surfaces," J. Opt. Soc. Am. **A2**, 2274–2284 (1985).
[21]R. L. Holford, "Scattering of sound waves at a periodic, pressure-release surface: An exact solution," J. Acoust. Soc. Am. **70**, 1116–1128 (1981).
[22]W. C. Meecham, "On the use of the Kirchhoff approximation for the solution of reflection problems," J. Rational Mech. Anal. **5**, 323–334 (1956).
[23]J. J. Dongarra, J. R. Bunch, C. B. Moler, and G. W. Stewart, LINPACK *Users' Guide* (Society for Industrial and Applied Mathematics, Philadelphia, 1979).
[24]L. D. Landau and E. M. Lifshitz, *Fluid Mechanics* (Pergamon, Oxford, 1959), p. 251.
[25]The spectral method has been found more convenient, especially for surface derivatives, than the autoregressive (AR) method used in Ref. 30. In this paper, the AR method was used for just one set of surfaces (Figs. 5–7).
[26]M. B. Priestly, *Spectral Analysis and Time Series* (Academic, New York, 1981), p. 208.
[27]D. E. Barrick, "Rough surface scattering based on the specular point theory," IEEE Trans. Antennas Propag. **AP-16**, 447–454 (1968).
[28]C. T. H. Baker, *The Numerical Treatment of Integral Equations* (Clarendon, Oxford, 1977), pp. 635–684.
[29]E. I. Thorsos, "The validity of the Kirchhoff approximation for rough surface scattering using a Gaussian roughness spectrum—extended version," unpublished manuscript, 27 August 1987.
[30]E. I. Thorsos, "Exact numerical methods versus the Kirchhoff approximation for rough surface scattering," in *Computational Acoustics*, Vol. II. *Algorithms and Applications*, edited by D. Lee, R. L. Sternberg, and M. H. Schultz (North-Holland, Amsterdam, 1988).
[31]A. Ishimaru, *Wave Propagation and Scattering in Random Media* (Academic, New York, 1978), Vol. II, Chap. 21; this reference uses the "radar cross section," which differs by a factor of 2π from the definition used here for 1-D surfaces (4π for 2-D surfaces).
[32]R. A Brockelman and T. Hagfors, "Note on the effect of shadowing on the backscattering of waves from the random rough surface," IEEE Trans. Antennas Propag. **AP-14**, 621–629 (1966).
[33]P. J. Lynch, "Curvature corrections to rough-surface scattering at high frequencies," J. Acoust. Soc. Am. **47**, 804–815 (1970).
[34]The quantity $\langle R^2 \rangle^{1/2}$ with R given by (34) is not well defined for a random surface, since occasionally $d^2f/dx^2 \cong 0$. As an alternative, we define the "rms radius of curvature" to be the reciprocal of the rms curvature $\tilde{R} \equiv \langle 1/R^2 \rangle^{-1/2}$, with R given by (34). Direct evaluation using surface realizations shows (36) to be an accurate estimate of this definition to within a few percent.
[35]For correspondence with Eq. 21-63 of Ref. 31, differences in angle and cross-section definitions and spectral density normalization must be taken into account.